Efficient Ca^{2+} buffering in fast-spiking basket cells of rat hippocampus

Yexica Aponte, Josef Bischofberger and Peter Jonas

Physiological Institute I, University of Freiburg, Hermann-Herder-Str. 7, D-79104 Freiburg, Germany

Fast-spiking parvalbumin-expressing basket cells (BCs) represent a major type of inhibitory interneuron in the hippocampus. These cells inhibit principal cells in a temporally precise manner and are involved in the generation of network oscillations. Although BCs show a unique expression profile of Ca^{2+}-permeable receptors, Ca^{2+}-binding proteins and Ca^{2+}-dependent signalling molecules, physiological Ca^{2+} signalling in these interneurons has not been investigated. To study action potential (AP)-induced dendritic Ca^{2+} influx and buffering, we combined whole-cell patch-clamp recordings with ratiometric Ca^{2+} imaging from the proximal apical dendrites of rigorously identified BCs in acute slices, using the high-affinity Ca^{2+} indicator fura-2 or the low-affinity dye fura-FF. Single APs evoked dendritic Ca^{2+} transients with small amplitude. Bursts of APs evoked Ca^{2+} transients with amplitudes that increased linearly with AP number. Analysis of Ca^{2+} transients under steady-state conditions with different fura-2 concentrations and during loading with 200 μM fura-2 indicated that the endogenous Ca^{2+}-binding ratio was $\sim$200 ($\kappa_S = 202 \pm 26$ for the loading experiments). The peak amplitude of the Ca^{2+} transients measured directly with 100 μM fura-FF was 39 nM AP^{-1}. At $\sim$23°C, the decay time constant of the Ca^{2+} transients was 390 ms, corresponding to an extrusion rate of $\sim$600 s^{-1}. At 34°C, the decay time constant was 203 ms and the corresponding extrusion rate was $\sim$1100 s^{-1}. At both temperatures, continuous theta-burst activity with three to five APs per theta cycle, as occurs *in vivo* during exploration, led to a moderate increase in the global Ca^{2+} concentration that was proportional to AP number, whereas more intense stimulation was required to reach micromolar Ca^{2+} concentrations and to shift Ca^{2+} signalling into a non-linear regime. In conclusion, dentate gyrus BCs show a high endogenous Ca^{2+}-binding ratio, a small AP-induced dendritic Ca^{2+} influx, and a relatively slow Ca^{2+} extrusion. These specific buffering properties of BCs will sharpen the time course of local Ca^{2+} signals, while prolonging the decay of global Ca^{2+} signals.

(Received 30 October 2007; accepted after revision 11 February 2008; first published online 14 February 2008)
Corresponding author P. Jonas: Physiological Institute I, University of Freiburg, Hermann-Herder-Str. 7, D-79104 Freiburg, Germany. Email: peter.jonas@physiologie.uni-freiburg.de

GABAergic interneurons are essential for information processing in cortical neuronal networks. Within this group of morphologically and functionally diverse cell types (Freund & Buzsáki, 1996; Somogyi & Klausberger, 2005), fast-spiking parvalbumin-expressing basket cells (BCs) are thought to have particularly important functions. These interneurons represent the most abundant interneuron subtype, corresponding to $\sim$20% of all GABAergic interneurons in the hippocampus (Freund & Buzsáki, 1996). BCs have an extensive axonal arborization, by which they innervate a large number of target neurons. BCs also generate large inhibitory postsynaptic conductances in their target cells (Kraushaar & Jonas, 2000). Furthermore, BCs mainly contact the perisomatic region of postsynaptic neurons, permitting efficient control of action potential (AP) initiation in the axon initial segment and proximal axon (Cobb *et al.* 1995). These specialized properties allow BCs to efficiently participate in feedforward and feedback inhibition (Pouille & Scanziani, 2004).

Previous studies revealed that BCs show fast electrical signalling at multiple levels (Jonas *et al.* 2004). BCs receive a fast excitatory synaptic input, which allows them to detect coincident excitation of pyramidal neurons (Miles, 1990; Geiger *et al.* 1997; Galarreta & Hestrin, 2001). BCs are able to generate high-frequency trains of APs during sustained current injection *in vitro* (Rudy & McBain, 2001) and during theta–gamma activity *in vivo* (Bragin *et al.* 1995;

 DOI: 10.1113/jphysiol.2007.147298

Penttonen *et al.* 1998; Csicsvari *et al.* 2003). Finally, BCs generate rapid inhibitory output signals in their target cells, especially if the postsynaptic neuron is another BC (Bartos *et al.* 2007). Rapid signalling in BCs appears to be essential for both the fast inhibition of principal neuron ensembles and the generation of network oscillations in the gamma frequency range (30–90 Hz; Jonas *et al.* 2004; Bartos *et al.* 2007).

Whereas a large amount of information is available on electrical signalling in BCs, Ca^{2+} signalling in these interneurons has remained largely uncharacterized. However, indirect evidence suggests that the properties of Ca^{2+} signalling in BCs may be distinct from those of principal cells or other interneuron subtypes. First, BCs selectively express Ca^{2+}-permeable glutamate receptors of the L-α-amino-3-hydroxy-5-methyl-4-isoxazolepropionate (AMPA) subtype (Koh *et al.* 1995; Geiger *et al.* 1995; Toth *et al.* 2000; Lei & McBain, 2002; Goldberg *et al.* 2003*b*). Second, BCs selectively express the Ca^{2+}-binding protein parvalbumin. However, the contribution of this Ca^{2+}-binding protein to endogenous Ca^{2+} signalling is unknown, since parvalbumin binds Ca^{2+} slowly in the presence of physiological Mg^{2+} concentrations (Schwaller *et al.* 2002; Müller *et al.* 2007). Third, BCs differ from principal cells in the expression of Ca^{2+}-dependent signalling molecules. For example, BCs lack the expression of the α subunit of calcium-calmodulin-dependent kinase II and calcineurin (Sík *et al.* 1998). Finally, BCs express distinct forms of Ca^{2+}-dependent synaptic plasticity at their glutamatergic input synapses (Kullmann & Lamsa, 2007). However, a quantitative analysis of Ca^{2+} buffering in identified BCs has not been performed. Understanding the Ca^{2+} buffering in interneurons may be also important to understand the selective resistance or vulnerability of these neurons under pathophysiological conditions (Sloviter *et al.* 2003).

To determine the endogenous Ca^{2+} buffering in rigorously identified BCs, we combined whole-cell patch-clamp recordings with ratiometric Ca^{2+} imaging at proximal apical dendrites, using both the high-affinity indicator fura-2 and the low-affinity dye fura-FF. The goal was to determine the endogenous Ca^{2+}-binding ratio (i.e. the ratio of buffer-bound Ca^{2+} changes over free Ca^{2+} changes; Neher & Augustine, 1992; Neher, 1998), the amplitude of the Ca^{2+} transient evoked by single APs in the absence of exogenous buffers, and the Ca^{2+} extrusion rate. Our results reveal that, in comparison to pyramidal neuron dendrites (Helmchen *et al.* 1996), BC dendrites show a high endogenous Ca^{2+}-binding ratio. Although BCs are coincidence detectors at the level of synaptic currents and potentials (Geiger *et al.* 1997; Galarreta & Hestrin, 2001), they behave as integrators at the level of AP-induced Ca^{2+} signals. A preliminary account of the data was published in abstract form (Aponte *et al.* 2006*a*).

Methods

Patch-clamp recording from basket cells in hippocampal slices

Transverse 300-μm-thick slices were cut from the hippocampus of 18- to 21-day-old Wistar rats using a commercial (Dosaka, Kyoto, Japan) or a custom-built vibratome (Geiger *et al.* 2002). Animals were killed by rapid decapitation without anaesthesia in accordance with national and institutional guidelines. Experiments were approved by the Animal Care Committee Freiburg according to §15 of the Tierschutzgesetz (registry T-04/10). Slices were kept at 35°C for 30 min after slicing and then at room temperature in physiological extracellular saline containing (mM): 125 NaCl, 25 $NaHCO_3$, 2.5 KCl, 1.25 NaH_2PO_4, 2 $CaCl_2$, 1 $MgCl_2$ and 25 glucose, equilibrated with 95% O_2–5% CO_2. Dentate gyrus basket cells were tentatively identified by the size and the location of the soma at the granule cell layer–hilus border using infrared differential interference contrast (IR-DIC) videomicroscopy (Koh *et al.* 1995; Aponte *et al.* 2006*b*).

Patch pipettes were pulled from borosilicate glass tubing (2.0 mm outer diameter, 1.0 mm inner diameter; Hilgenberg, Malsfeld, Germany). A Multiclamp 700A amplifier (Molecular Devices, Palo Alto, CA, USA) was used for current-clamp recordings. Series resistance (5–15 MΩ) was compensated by the bridge-balance circuit of the amplifier. The resting membrane potential measured after obtaining a whole-cell recording was between −65 and −54 mV and was set to −70 mV (membrane potential values uncorrected for liquid junction potentials) by injecting a constant negative holding current (< 150 pA). Voltage signals were filtered at 4 kHz with a 4-pole low-pass Bessel filter and sampled at 10 kHz. Pulse generation and data acquisition was performed using FPulse (U. Fröbe, Physiological Institute) running under Igor Pro 5.01 (Wavemetrics, Lake Oswego, OR, USA) on a personal computer, which controlled a 1401plus interface (CED, Cambridge, UK).

To obtain somatic whole-cell recordings, we used patch pipettes (2–4 MΩ) filled with internal solution containing (mM): 125 potassium gluconate, 4 $MgCl_2$, 4 K_2ATP, 0.3 NaGTP, 10 Na_2-phosphocreatine and 10 Hepes, different concentrations of Ca^{2+} indicator dyes, and 0.2% biocytin (pH adjusted to 7.2 with KOH). Free ATP concentration in this solution was estimated as 0.63 mM. Action potential (AP) patterns were determined in the current-clamp configuration using 1 s depolarizing current pulses. Only fast-spiking neurons with an average AP frequency larger than 50 Hz were used for subsequent Ca^{2+} imaging experiments. Recordings were made at 22–24°C, unless specified differently.

Fluorescence measurements with fura-2 and fura-FF

For the measurement of the intracellular Ca^{2+} signals, different concentrations of fura-2 or fura-FF (Invitrogen, Eugene, OR, USA; Neher, 1995) were added to the pipette solution. The excitation light source (Polychrome I with 75 W xenon lamp, Till Photonics, Munich, Germany) was coupled to the epifluorescent port of the microscope (Axioskop FS2, Zeiss, Göttingen, Germany; 60× water immersion objective, Olympus, Tokio, Japan) via a light guide. Light intensity was adjusted to minimize bleaching of the fluorescent dyes, which was $\sim 0.2 \pm 0.1\%$ ($n = 7$) during a 5 s sweep, estimated as the decrease of fluorescence emission with excitation at the isosbestic wavelength of 356 nm (the Ca^{2+}-insensitive wavelength under our experimental conditions). The filter combination for excitation and emission comprised a beam splitter (BSP400) and an emission filter (BP430-630; AHF Analysentechnik Tübingen, Germany).

Fluorescence was measured with a backilluminated frame-transfer charge-coupled device (CCD) camera (EBFT 512, Princeton Instruments, Trenton, NJ, USA). Images with full spatial resolution were taken with exposure times of 5 s. For high-speed Ca^{2+} measurements (100 Hz sample frequency), a rectangular region of interest (ROI) was defined over the proximal apical dendrite of a BC (typical size 5 μm × 20 μm) at a distance of 10–60 μm from the border of the soma. Fluorescence measurements were initiated ~10 min after the whole-cell configuration was obtained, with the exception of loading curve experiments in which measurements were started immediately after breaking in (Fig. 5). Fluorescence traces had a duration of 5–30 s and were separated by intersweep intervals of 10–30 s. Signals were corrected for background, which was obtained from a second ROI with identical size but shifted 10–15 μm perpendicularly to the dendritic axis in comparison to the original ROI (Normann *et al.* 2000). The pixels included in the two ROIs were binned on-chip and digitized subsequently by the camera controller (Micromax, 1 MHz, Princeton Instruments). Image acquisition was controlled using custom-made programs written in Visual Basic running under WinView 32 (Princeton Instruments). For display purposes, a subset of traces with fura-FF was digitally filtered at a cutoff frequency of 15 Hz.

Calibration of the Ca^{2+} measurements

To convert the fluorescence signals into Ca^{2+} concentrations, we used isosbestic ratioing (Neher & Augustine, 1992; Schiller *et al.* 1995; Normann *et al.* 2000). The AP-induced fluorescence change was recorded at an excitation wavelength of 380 nm. The isosbestic fluorescence was measured immediately before and after each sweep, using the Ca^{2+}-insensitive excitation wavelength of 356 nm. The ratio of the background-corrected fluorescence signals $R = F_{356}/F_{380}$ was calculated, and converted into the Ca^{2+} concentration using the equation (Grynkiewicz *et al.* 1985):

$$[Ca^{2+}] = K_{eff}(R - R_{min})/(R_{max} - R), \quad (1)$$

with $K_{eff} = K_d\,(R_{max}/R_{min})$, where K_d is the dissociation constant, R_{min} the ratio in Ca^{2+}-free solution and R_{max} the ratio when the Ca^{2+} indicator is completely saturated with Ca^{2+}. These values were determined directly in BCs with internal solutions containing either 10 mM EGTA (Ca^{2+} free), 30 mM $CaCl_2$ (maximal Ca^{2+}) or a mixture of 7.06 mM CaEGTA and 2.94 mM EGTA (Ca^{2+} calibration kit, Invitrogen), resulting in a free Ca^{2+} concentration of 400 nM. Using these solutions, the values for fura-2 were $R_{min} = 0.72 \pm 0.01$ ($n = 11$), $R_{max} = 4.83 \pm 0.08$ ($n = 6$), and $R_{400} = 1.41 \pm 0.03$ ($n = 9$) resulting in a K_d of 297 nM. The corresponding values for fura-FF were $R_{min} = 0.60 \pm 0.01$ ($n = 16$), $R_{max} = 4.30 \pm 0.06$ ($n = 7$), and $R_{400} = 0.65 \pm 0.01$ ($n = 8$), corresponding to a K_d of 4.18 μM.

'Single compartment' model of dendritic Ca^{2+} buffering

To analyse the dendritic Ca^{2+} buffering properties in BCs, a 'single compartment' approach was used, assuming that reactions between Ca^{2+} and buffers are instantaneous and buffers are non-saturable (Neher & Augustine, 1992; Helmchen *et al.* 1996, 1997; Neher, 1998). The fraction of Ca^{2+} which binds to endogenous Ca^{2+} buffers (S) during the Ca^{2+} influx evoked by a short AP can be quantified by the endogenous Ca^{2+}-binding ratio, which is defined as

$$\kappa_S = \Delta[SCa]/\Delta[Ca^{2+}], \quad (2)$$

where ΔSCa represents the increase in buffer-bound Ca^{2+} and ΔCa^{2+} the increase in the free Ca^{2+} concentration (Neher & Augustine, 1992). Similarly the Ca^{2+}-binding ratio of the exogenous buffer fura-2 (B) can be expressed as $\kappa_B = \Delta[BCa]/\Delta[Ca^{2+}]$. Assuming that the intracellular Ca^{2+} concentration within a dendritic compartment, corresponding to a recorded ROI, is homogenously elevated during an AP from a resting level $[Ca^{2+}]_1$ to a peak level $[Ca^{2+}]_2$, the exogenous binding ratio can be calculated according to the law of mass action as

$$\kappa_B = B_t K_d \big/ \big(([Ca^{2+}]_2 + K_d)([Ca^{2+}]_1 + K_d)\big), \quad (3)$$

where B_t and K_d represent the total concentration and the Ca^{2+} dissociation constant of fura-2, respectively (Neher & Augustine, 1992). If we assume that a total amount of calcium $Ca^{2+}{}_t$ enters a dendritic compartment with volume V and instantaneously binds to the different buffers, it will increase the free Ca^{2+} concentration ($\Delta[Ca^{2+}]_i$), the Ca^{2+}-bound fraction of fura-2 (Δ[BCa]),

and the Ca^{2+}-bound fraction of the endogenous Ca^{2+} buffers (Δ[SCa]) according to the relationship

$$Ca^{2+}{}_t/V = \Delta[Ca^{2+}]_i + \Delta[BCa] + \Delta[SCa] \quad (4)$$

Using the definition of the Ca^{2+} binding ratios, eqn (4) can be rewritten as

$$\Delta[Ca^{2+}]_t = \Delta[Ca^{2+}]_i(1 + \kappa_B + \kappa_S), \quad (5)$$

where $\Delta[Ca^{2+}]_t = Ca^{2+}{}_t/V$. With $A^{-1} = 1/\Delta[Ca]_i$, eqn (5) can be rearranged as

$$A^{-1} = (1 + \kappa_B + \kappa_S)/\Delta[Ca^{2+}]_t \quad (6)$$

Thus, A^{-1} plotted against κ_B should follow a straight line, which intercepts the horizontal axis at $-(1 + \kappa_S)$. Using this relationship, it is therefore possible to estimate the endogenous Ca^{2+}-binding ratio κ_S by measuring the amplitude of the Ca^{2+} transients with different concentrations of fura-2 (leading to different values for κ_B according to eqn (3)). Furthermore, the amplitude of Ca^{2+} transients in the absence of fura-2 can be obtained by extrapolation to $\kappa_B = 0$. Although the described approach is strictly valid only for rapidly binding buffers, the additional presence of a slow buffer will primarily interfere with the decay time course, but not with the peak amplitude. Therefore, we determined the endogenous binding ratio using peak amplitudes rather than decay time constants (Lee *et al.* 2000*b*).

The amplitude of the Ca^{2+} transient in the absence of exogenous buffers was also approximated by measurement of Ca^{2+} transients with 100 μM of the low-affinity Ca^{2+} indicator fura-FF. For $[Ca^{2+}] \ll K_d$, the exogenous Ca^{2+} binding ratio can be estimated as $\kappa_B = [\text{fura-FF}]/K_d = 100/4.18 = 24$, an order of magnitude smaller than the endogenous binding ratio κ_S. Finally, the lumped Ca^{2+} extrusion rate (γ) comprising both Ca^{2+} extrusion across the plasma membrane and uptake into organelles was calculated from the decay time constant (τ_w) measured with fura-FF as

$$\gamma = (1 + \kappa_B + \kappa_S)/\tau_w; \quad (7)$$

the factor $(1 + \kappa_B + \kappa_S)$ arises because for constant extrusion rate, the decay time constant scales linearly with the amount of buffer-bound Ca^{2+} (Helmchen & Tank, 2005).

Post hoc visualization of morphology and immunocytochemistry

For morphological identification of BCs, neurons were filled with biocytin. After ~20–30 min recording, slices were fixed overnight with 4% paraformaldehyde in phosphate-buffered solution (PBS; 0.1 M, pH 7.3). Following wash with PBS, slices were incubated with FITC-conjugated avidin-D (Vector Laboratories, Burlingame, CA, USA) in PBS and 0.3% triton X-100 overnight at 4°C. After wash, slices were embedded in Prolong Gold Antifade (Invitrogen). Labelled neurons were examined either by epifluorescence or with a confocal laser-scanning microscope (LSM 510, Zeiss). Only cells with an axonal arborization confined to the granule cell layer (> 90%) were included in this study.

Additionally, a subset of BCs was examined for the expression of the Ca^{2+}-binding protein parvalbumin. Slices were incubated with 10% goat serum for 1 h and subsequently with a primary monoclonal antibody against PV (mouse, Swant, Bellinzona, Switzerland, 1 : 10000) in PBS containing 5% goat serum and 0.3% triton X-100 for 20–24 h at 22°C. The secondary antibody (goat anti-mouse, Alexa 568, 1 : 500, Invitrogen) was applied together with FITC-conjugated avidin-D in PBS and 0.3% triton X-100 at 4°C overnight. From a sample of 60 BCs examined by immunochemistry, 27 were immunopositive for parvalbumin, consistent with partial preservation of parvalbumin in the whole-cell recorded neurons.

Data analysis and statistics

Ca^{2+} transients were analysed with procedures running under Igor Pro. The peak amplitude of the AP-induced Ca^{2+} transient was measured as the difference between baseline and the absolute maximum during the trace; the maximum typically occurred shortly after the last AP in the train stimulation. The decay time course of the AP-induced Ca^{2+} transients were fitted with either a single exponential or the sum of two exponentials $y(t) = A_1 \exp(-t/\tau_1) + A_2 \exp(-t/\tau_2)$, and the amplitude-weighted time constant was calculated as $\tau_w = (A_1 \tau_1 + A_2 \tau_2)/(A_1 + A_2)$. The A^{-1} *versus* κ_B relationship was analysed by unweighted linear regression according to eqn (6). Traces of Ca^{2+} transients in the figures represent averages of 5 to 10 consecutive sweeps, unless specified differently. Values indicate mean ± S.E.M. Error bars in figures also represent S.E.M. Statistical significance was tested by a non-parametric Mann–Whitney or Kruskal–Wallis test at the significance level (P) indicated, using Graphpad Prism 3.0 (Graphpad Inc., San Diego, CA, USA). Confidence intervals of estimates of κ_S from population data were obtained by bootstrap procedures implemented in Mathematica 4.1 (Wolfram Research, Champaign, IL, USA; see Efron & Tibshirani, 1998). 1000 artificial data sets were generated from the means and SEMs of the original data set using normally distributed random numbers, and analysed as the original.

Results

Ca^{2+} signalling in apical dendrites of BCs

To analyse the endogenous Ca^{2+} buffering in BCs, we combined whole-cell patch-clamp recordings with

ratiometric Ca^{2+} imaging in proximal apical dendrites. BCs were rigorously identified on the basis of their appearance in the IR-DIC image (Fig. 1*A*), the fast-spiking action potential (AP) phenotype (Fig. 1*B*), and the location of the axonal arborization, which was visualized by biocytin labelling in all recorded cells (Fig. 1*C*). Furthermore, the expression of the Ca^{2+}-binding protein parvalbumin was examined in a subset of recorded neurons (Fig. 1*D*). Only neurons that generated > 50 APs per second during sustained current injection and showed an axon with $> 90\%$ of collaterals in the granule cell layer were used for subsequent analysis.

To characterize Ca^{2+} signalling in BCs, we first recorded Ca^{2+} transients in the proximal apical dendrites of BCs with the high-affinity indicator dye fura-2 (Fig. 2*A*). With 100 μM fura-2, the resting Ca^{2+} concentration was 71 ± 7 nM ($n = 41$). Single APs evoked Ca^{2+} transients with a peak amplitude of 22 ± 1 nM ($n = 30$; Fig. 2*B*). In contrast, 50 or 100 Hz trains of 10 APs evoked Ca^{2+} transients with larger peak amplitude of 208 ± 19 nM under identical conditions (Fig. 2*C*). We then fitted the decay time course of Ca^{2+} transients with mono- and biexponential functions (Collin *et al.* 2005). A biexponential fit was preferred if both fast and slow components had amplitude contributions of $> 10\%$. Using this criterion, Ca^{2+} transients were considered biexponential in 25 of 30 BCs for single APs and 22 of 22 BCs for 10 APs. On average, the fast time constant (τ_1) was 300 ± 33 ms (49% amplitude contribution) and the slow time constant (τ_2) was 1926 ± 155 ms for single APs, resulting in an amplitude-weighted decay time constant (τ_w) of 980 ± 69 ms. For a train of 10 APs, the corresponding values were $\tau_1 = 395 \pm 32$ ms (62% amplitude contribution), $\tau_2 = 1915 \pm 144$ ms and $\tau_w = 991 \pm 96$ ms. The peak amplitude of the Ca^{2+} transients in the proximal apical dendrite was constant over time (Fig. 2*D*, upper panel) and was not significantly dependent on the distance in the range of $\sim$10–60 μm from the soma ($P > 0.5$; Fig. 2*D*, lower panel), indicating stationarity and spatial homogeneity.

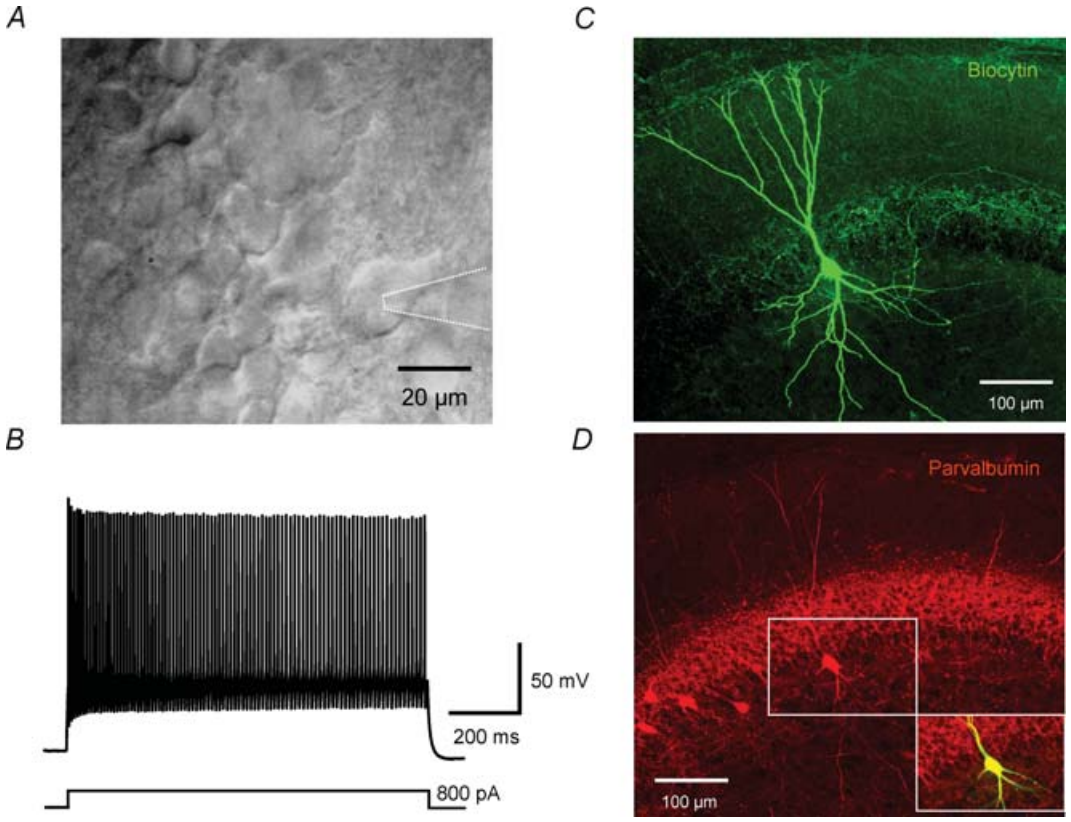

Figure 1. Identification of parvalbumin-expressing, fast-spiking basket cells in the dentate gyrus
A, infrared differential interference contrast videomicroscopy image of a BC near the border between granule cell layer and hilus. Dotted lines indicate recording pipette. *B*, fast-spiking AP phenotype of the same BC recorded in the current-clamp configuration during a 800 pA, 1 s current pulse. The mean action potential frequency in this cell was 94 Hz. *C*, confocal stack projection of a BC filled with biocytin and stained with FITC-conjugated avidin. The axon is mainly located in the granule cell layer. *D*, immunohistochemistry of the same BC with an antibody against parvalbumin. Inset: overlay of biocytin signal and parvalbumin immunoreactivity, showing that the recorded cell is parvalbumin positive.

To examine whether Ca^{2+} transients evoked by single APs summated linearly, we compared peak amplitude and kinetics of Ca^{2+} transients evoked by bursts of different numbers of stimuli (Fig. 3). As the number of APs was increased from 1 to 30, the amplitude of the Ca^{2+} transients became markedly larger (Fig. 3*A* and *B*). Quantitative analysis revealed that the amplitude of the Ca^{2+} transient was proportional to the number of spikes (Fig. 3*B*). In contrast, the amplitude-weighted average decay time constants τ_w of the Ca^{2+} transients were not significantly dependent on the number of spikes ($P > 0.1$; Fig. 3*C*). In conclusion, the amplitude of the Ca^{2+} transients evoked by a burst of APs was proportional to the number of APs, whereas the decay of the Ca^{2+} transients was independent of AP number. These results were consistent with linear Ca^{2+} signalling in the proximal dendrites of BCs.

Endogenous Ca^{2+}-binding ratio under steady-state conditions and during indicator loading

To quantify the endogenous buffer capacity of BCs, we took advantage of the competition between endogenous buffers and exogenous Ca^{2+} indicators. BCs were loaded with either 50, 100 or 200 μM fura-2, and Ca^{2+} transients evoked by a burst of five APs were measured under steady-state conditions 10–20 min after the whole-cell recording configuration was obtained (Fig. 4). Ca^{2+} transients recorded with different concentrations of fura-2 showed significantly different peak amplitudes and time

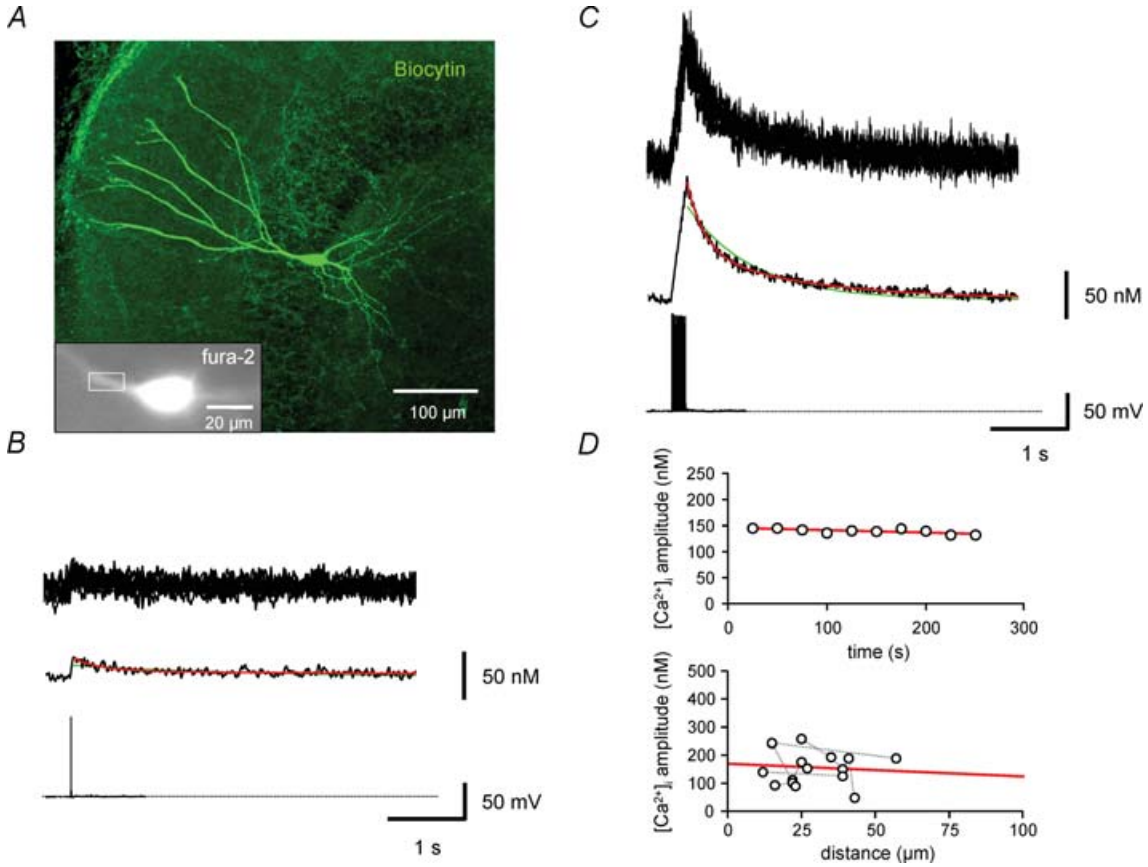

Figure 2. Ca^{2+} transients in proximal apical dendrites of BCs evoked by single spikes and trains of APs
A, fluorescence image of a BC filled with 100 μM fura-2 (excitation wavelength 380 nm), shown together with an overview of the morphology of the same cell filled with biocytin and stained with FITC-conjugated avidin (large image). Rectangle indicates the region of interest used for imaging of Ca^{2+} transients. *B* and *C*, Ca^{2+} transients in the proximal apical dendrite evoked by single APs (*B*) or trains of 10 APs at 50 Hz (*C*). Upper traces, single consecutive sweeps; middle traces, average of 10 sweeps; lower traces, corresponding APs evoked by brief current pulses. Green curves represent monoexponential fits, red curves biexponential fits to the decay phase of the Ca^{2+} transients. Data in *A*–*C* were obtained from the same BC. *D*, plot of peak amplitude of Ca^{2+} transient against recording time in the same cell shown in *A*–*C* (upper graph) and against distance (measured from the border of the soma to the centre of the region of interest) in a subset of BCs in which measurements were made at multiple distances. Data from the same cell are connected by gray dotted lines. Continuous red lines represent the results of linear regression.

courses (Fig. 4*A*). The peak amplitudes were 125 ± 13 nM, 83 ± 8 nM and 66 ± 7 nM with 50, 100 and 200 μM fura-2, respectively ($P < 0.01$; Fig. 4*B*, upper panel). Likewise, the corresponding amplitude-weighted average decay time constants τ_w were 833 ± 81 ms, 1291 ± 119 ms and 2171 ± 166 ms ($P < 0.001$; Fig. 4*B*, lower panel). Both the reduction in peak amplitude and the prolongation of the decay time course with increasing concentration of fura-2 indicate competition of the Ca^{2+} indicator dye with endogenous buffers.

To determine the endogenous Ca^{2+}-binding ratio (Neher & Augustine, 1992), we plotted the inverse of the peak amplitude of the Ca^{2+} transients against the exogenous Ca^{2+}-binding ratio (κ_B), which was calculated from the fura-2 concentration according to eqn (3). In the framework of a single-compartment model, the relation between A^{-1} and κ_B is expected to fall on a straight line (eqn (6)). Therefore, data points from a population of 66 recorded BCs were fitted by linear regression and the endogenous Ca^{2+}-binding ratio κ_S was obtained from the intercept of the fitted line with the horizontal axis. Analysis of mean values for the three fura-2 concentrations gave a κ_S value of 214. Because of the cell–cell variability of the data (Fig. 4*C*), the statistical reliability of the estimate of κ_S was addressed using a bootstrap method. This analysis revealed that the 15.9–84.1% confidence interval (corresponding to the standard deviation of a normally distributed variable) was [138, 355] (Fig. 4*D*). These values are markedly larger than the Ca^{2+}-binding ratios in the apical dendrites of cortical pyramidal cells determined with the same methods (64–90; Helmchen *et al.* 1996).

As Ca^{2+} transients were measured under steady-state conditions 10–20 min after the whole-cell configuration had been obtained, mobile buffers are expected to be largely washed out by cell dialysis (Schmidt *et al.* 2003). Thus, the Ca^{2+}-binding ratio obtained under these conditions would be primarily determined by fixed buffers. To quantify the Ca^{2+}-binding ratio under conditions in which mobile buffers are better preserved, we performed Ca^{2+} indicator loading experiments (Fig. 5). Ca^{2+}

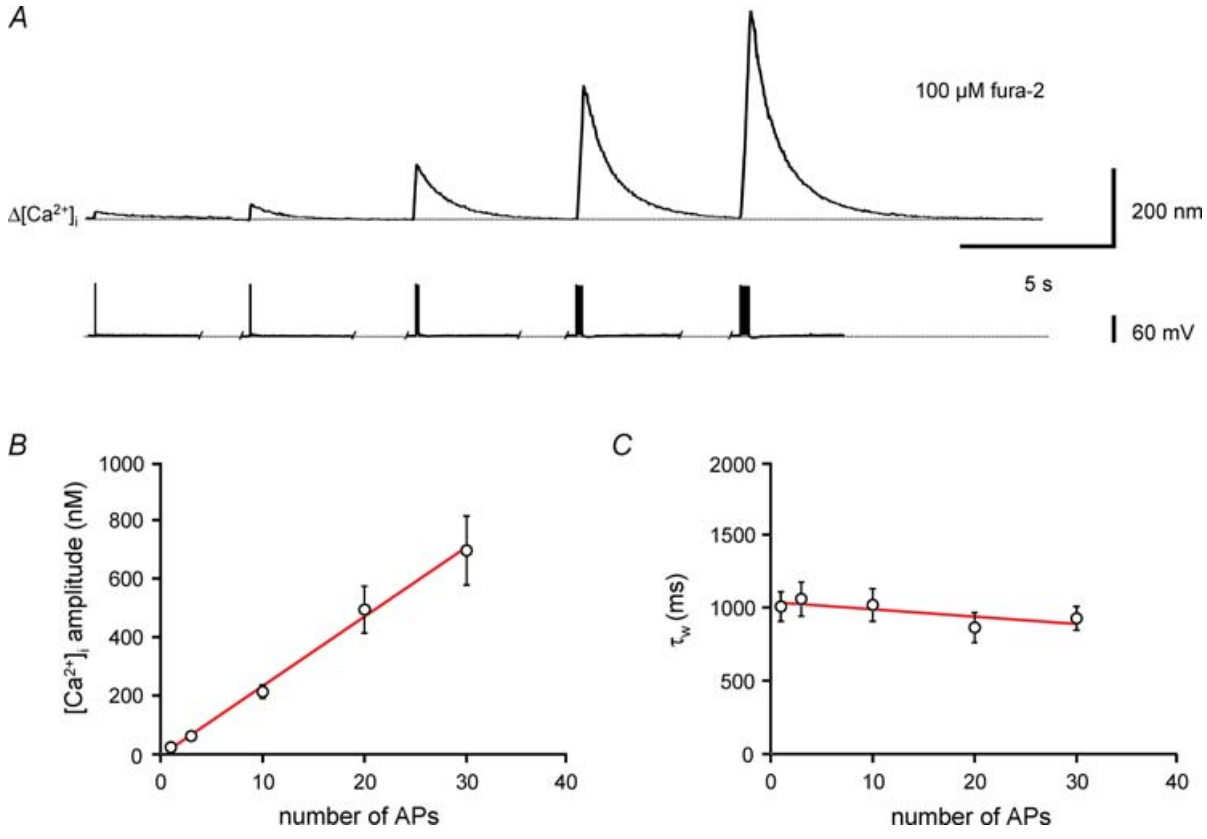

Figure 3. Linear summation of Ca^{2+} transients evoked by different numbers of action potentials
A, Ca^{2+} transients in the apical dendrite of a BC filled with 100 μM fura-2 evoked by a single AP or 100 Hz bursts of 3, 10, 20 and 30 APs. Upper traces, averages of 20 sweeps; lower traces, corresponding APs and trains of APs evoked by brief current pulses. *B*, plot of peak amplitude of Ca^{2+} transients against the number of APs. Continuous curve represents the results of linear regression, yielding a steepness of 24 nM AP^{-1}. *C*, plot of amplitude-weighted decay time constant (τ_w) of the Ca^{2+} transients against the number of APs. Note that τ_w is almost independent of the number of spikes. Continuous curve represents the results of linear regression, yielding a steepness of −5 ms AP^{-1}. Data from 18 BCs loaded with 100 μM fura-2.

transients were measured in the apical dendrites of BCs at different times after obtaining the whole-cell configuration with 200 μM fura-2 in the pipette solution. Ca^{2+} transients early in the loading procedure showed a large amplitude and a fast decay (Fig. 5*A*, upper trace). In contrast, Ca^{2+} transients recorded at later times showed a reduced amplitude and a prolonged decay (Fig. 5*A*, lower traces), again indicating competition between fura-2 and endogenous buffers.

For quantitative analysis, we determined the fura-2 concentration corresponding to different time points, assuming that the dye concentration in the proximal apical dendrite under steady-state conditions reached the concentration in the pipette (200 μM; Fig. 5*B*, upper graph). Next, we calculated the corresponding exogenous Ca^{2+}-binding ratio (κ_B) from the fura-2 concentration. Finally, we plotted the inverse of the peak amplitude of the Ca^{2+} transient (Fig. 5*B*, lower graph) against κ_B. In

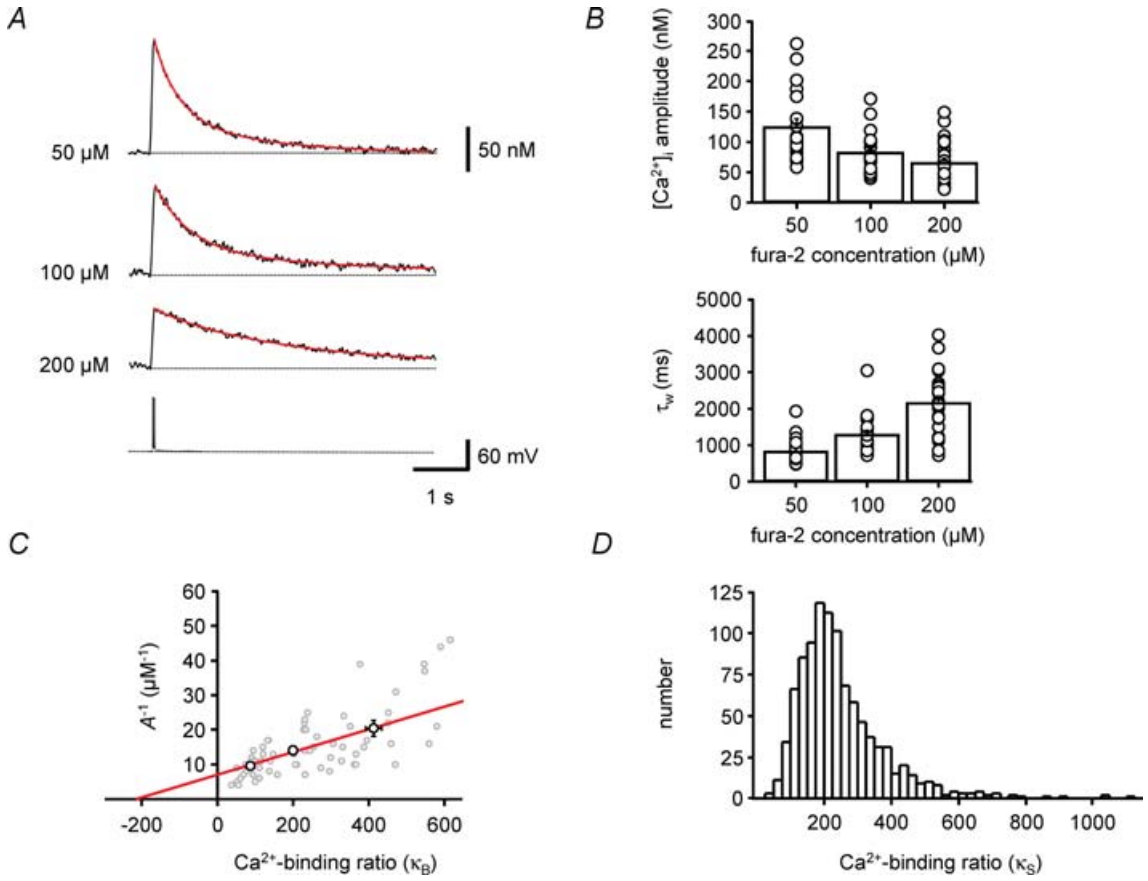

Figure 4. Estimation of endogenous Ca^{2+}-binding ratio by population analysis under steady-state conditions

A, Ca^{2+} transients evoked by 100 Hz bursts of 5 APs. Three different BCs were loaded with fura-2, with dye concentrations indicated on the left. Each Ca^{2+} transient trace is an average of 20 single sweeps. The lower trace represents the corresponding AP train. Red curves represent biexponential fits to the decay phase of the Ca^{2+} transients. Note that peak amplitude of the Ca^{2+} transients decreases, whereas the decay time constant increases with increasing concentration of fura-2, indicating competition between fura-2 and endogenous Ca^{2+} buffers. *B*, summary bar graphs showing the peak amplitude (upper graph) and amplitude-weighted decay time constant (τ_w, lower graph) of Ca^{2+} transients evoked by 100 Hz bursts of 5 APs at different concentrations of fura-2. Bars represent mean ± S.E.M.; circles represent data from individual BCs. *C*, plot of the inverse of the peak amplitude of Ca^{2+} transients against the exogenous Ca^{2+}-binding ratio, i.e. the Ca^{2+}-binding ratio of fura-2 (κ_B). κ_B was calculated from the fura-2 concentration according to eqn (3). Gray circles, data from 66 individual BCs; black circles, plot of mean values for 50, 100 and 200 μM fura-2. Continuous line represents the results of unweighted linear regression to the mean data. The endogenous Ca^{2+}-binding ratio (κ_S), estimated from the intercept of the fitted line with the horizontal axis, was 214. *D*, estimation of confidence intervals for κ_S. 1000 bootstrap replications of the original mean data were generated and corresponding κ_S values were determined by linear regression (see Methods). The histogram shows the distribution of estimated κ_S values. The 15.9–84.1% confidence interval was [138, 355]. Measurements were taken > 10 min after the whole-cell configuration was established.

the A^{-1} *versus* κ_B plot (Fig. 5*C*), data points on the left corresponded to early measurements, whereas data points on the right corresponded to late measurements in the loading experiment. Analysing the data by linear regression according to a single-compartment model revealed a mean endogenous Ca^{2+}-binding ratio κ_S of 202 ± 26 ($n = 7$; Fig. 5*D*; Table 1), very similar to that obtained from the mean population data under steady-state conditions (Fig. 4). The similarity of the values of κ_S obtained from the two data sets suggests that the endogenous Ca^{2+}-binding ratio in proximal apical dendrites of BCs is primarily determined by fixed buffers, whereas the contribution of mobile buffers is small. The value of κ_S in BCs obtained from loading experiments was larger than the values of κ_S estimated in cortical pyramidal cells with the same methods (126–168; Helmchen *et al.* 1996). In conclusion, analysis of population data under steady-state conditions and loading data under dynamic conditions indicate that the proximal apical dendrites of BCs show a large endogenous Ca^{2+}-binding ratio mainly determined by fixed buffers.

Amplitude of the Ca^{2+} transient and Ca^{2+} extrusion rate with minimal exogenous buffering

We next attempted to measure the amplitude of the minimally perturbed Ca^{2+} transient and the Ca^{2+} extrusion rate in the proximal apical dendrites of BCs. To

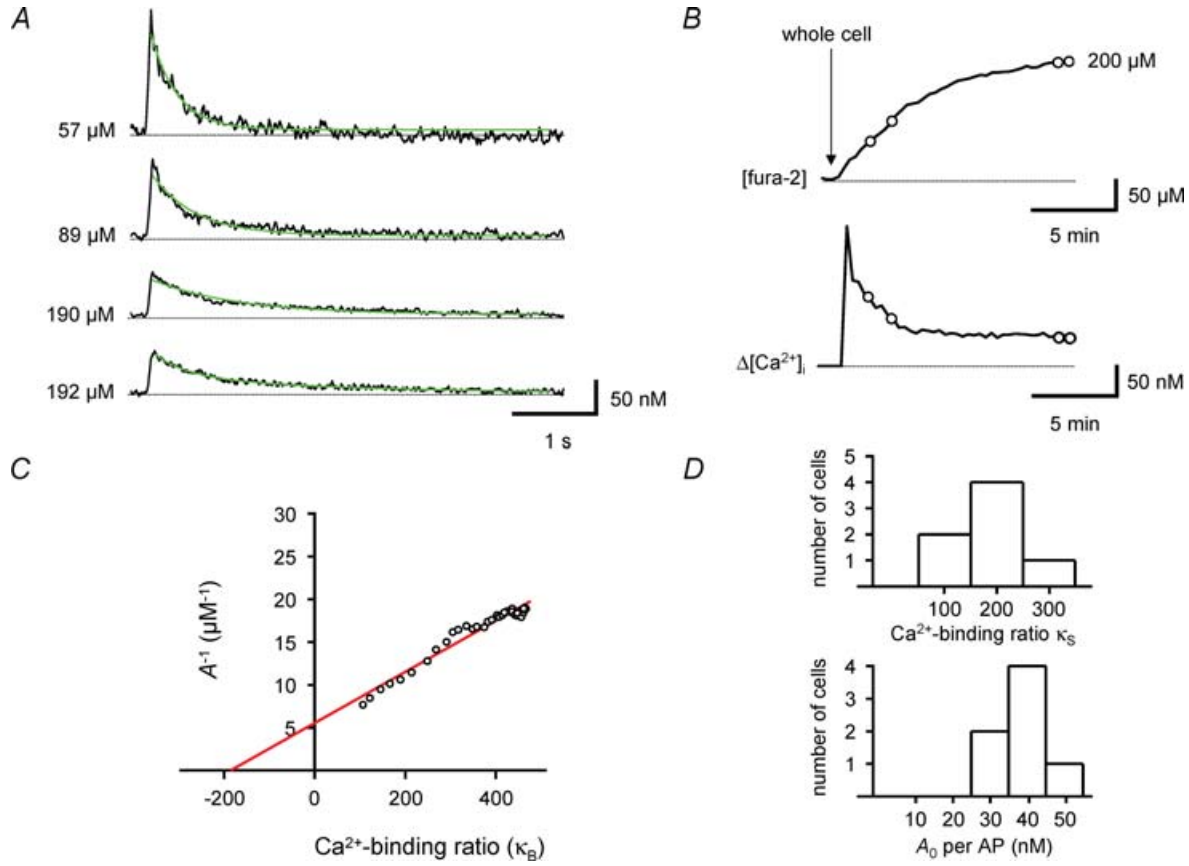

Figure 5. Estimation of endogenous Ca^{2+}-binding ratio during loading with the high-affinity indicator fura-2

A, single traces of Ca^{2+} transients recorded at different time points in a BC during loading with 200 μM fura-2, corresponding to different fura-2 concentrations in the dendrite (as indicated on the left of each trace). Green curves represent monoexponential fits to the decay phase of the Ca^{2+} transients. Note that the peak amplitude of the Ca^{2+} transients decreases, while the decay time constant increases during loading. *B*, plot of fura-2 concentration (upper trace) and simultaneously measured peak amplitude of Ca^{2+} transients (lower trace) before and after the whole-cell configuration was obtained. Circles indicate the data points corresponding to the traces shown in *A*. *C*, plot of the inverse of the peak amplitude of Ca^{2+} transients against exogenous Ca^{2+}-binding ratio, i.e. the Ca^{2+}-binding ratio of the indicator (κ_B). The continuous line represents the results of unweighted linear regression. The endogenous Ca^{2+}-binding ratio (κ_S), estimated from the intercept of the fitted line with the horizontal axis, was 186 in this BC. Data in *A*–*C* were obtained from the same cell. *D*, histograms of endogenous Ca^{2+}-binding ratio (κ_S, upper graph) and amplitude of dendritic Ca^{2+} transient per AP in the absence of fura-2 (A_0, lower graph) in 7 BCs. All experiments were performed with 100 Hz bursts of 5 APs.

Table 1. Summary of Ca^{2+} signalling properties of BCs determined with high- and low-affinity Ca^{2+} indicators

Parameter	Fura-2 (22–24°C)	Fura-FF (22–24°C)	Fura-FF (34°C)
Resting $[Ca^{2+}]_i$	71 ± 7 nM ($n = 41$)	—	—
κ_S (population analysis, steady state)	214 [138, 355] ($n = 66$)[1]	—	—
κ_S (loading experiments)	202 ± 26 ($n = 7$)[2]	—	—
$[Ca^{2+}]_i$ amplitude	43 ± 5 nM AP^{-1} ($n = 7$)[3]	39 nM AP^{-1} ($n = 7$)	22 nM AP^{-1} ($n = 12$)
Decay time constant τ_w	359 ± 38 ms ($n = 7$)[4]	390 ± 154 ms ($n = 7$)	203 ± 24 ms ($n = 12$)
$[Ca^{2+}]_i$ amplitude during theta–gamma burst stimulation	—	50 nM AP^{-1} ($n = 8$)[5]	37 nM AP^{-1} ($n = 7$)[5]

[1]Confidence interval was obtained by bootstrap analysis (Methods). [2]Standard error of the mean was calculated from all κ_S values obtained by separate analysis of each cell. [3]Value was obtained by extrapolation to $\kappa_B = 0$. [4]Value was obtained from early time points in the loading experiments ([fura-2] < 50 μM). [5]Values relate to the number of APs per burst.

minimize the interference of exogenous Ca^{2+} indicators with the Ca^{2+} transients, experiments were performed using the low-affinity indicator dye fura-FF (Fig. 6). Ca^{2+} transients were evoked by bursts of 1–30 APs (Fig. 6*A* and *B*). As found for fura-2, the amplitude of the Ca^{2+} transients increased proportionally to the number of APs in the burst (Fig. 6*C*). The slope of the relation between the peak amplitude of the Ca^{2+} transients and the number of APs was $A = 39$ nM AP^{-1}. With an exogenous Ca^{2+} binding ratio κ_B of 24 (for 100 μM fura-FF) and an endogenous Ca^{2+}-binding ratio κ_S of 202, this corresponds to a total Ca^{2+} load of $A^* (1 + \kappa_B + \kappa_S) = 8.9$ μM AP^{-1}. These values directly measured with the low-affinity dye fura-FF were in close agreement with the estimates obtained by extrapolation towards an exogenous Ca^{2+}-binding ratio of $\kappa_B = 0$ from the data measured with the high-affinity indicator fura-2 (43 ± 5 nM AP^{-1}; Fig. 5*D*; Table 1).

To determine the Ca^{2+} extrusion rate, we plotted the amplitude-weighted average decay time constant τ_w against the number of APs (Fig. 6*D*). τ_w was not significantly dependent on AP number, with a mean value of 390 ± 154 ms ($n = 7$; $P > 0.2$). These decay time constant values directly measured with the low-affinity indicator dye fura-FF were in close agreement with those obtained with the high-affinity indicator fura-2 at early time points in the loading experiment (Fig. 5*A*; Table 1). From the value of the decay time constant of the Ca^{2+} transients, the exogenous Ca^{2+}-binding ratio κ_B of 24 (for 100 μM fura-FF), and the endogenous Ca^{2+}-binding ratio κ_S of 202, the lumped Ca^{2+} extrusion rate comprising Ca^{2+} extrusion across the plasma membrane and uptake into organelles can be calculated from eqn (7) as $\gamma = 582\ s^{-1}$. Additional experiments at near-physiological temperature (34°C) gave a smaller amplitude, presumably caused by shortening of the action potential, and a faster decay of Ca^{2+} transients, probably caused by temperature dependence of extrusion (Fig. 6*C* and *D*). For 34°C, $A = 22$ nM AP^{-1} and $\tau_w = 203 \pm 24$ ms were obtained ($n = 12$; Table 1). Assuming that both exogenous and endogenous Ca^{2+}-binding ratio are independent of temperature, γ at 34°C can be calculated as $1118\ s^{-1}$. Thus, the extrusion rate in the proximal apical dendrites of BCs is slower than that in pyramidal cell dendrites ($1500–2000\ s^{-1}$; Helmchen *et al.* 1996; their Table 1).

Ca^{2+} signalling in proximal apical dendrites of BCs with physiological activity patterns

When a rat explores the environment, BCs *in vivo* generate APs in a theta–gamma-modulated manner, with two to five APs per theta cycle (Bragin *et al.* 1995; Penttonen *et al.* 1998; Csicsvari *et al.* 2003). To examine Ca^{2+} signalling during such behaviourally relevant protocols, we applied repetitive theta–gamma-burst stimulation and measured the resulting Ca^{2+} transients (Fig. 7). To minimize interference with exogenous Ca^{2+} indicators, these experiments were performed with the low-affinity indicator dye fura-FF.

Sustained theta-burst stimulation resulted in a long-lasting elevation in intracellular Ca^{2+} concentration in proximal apical dendrites of BCs due to temporal summation of Ca^{2+} transients generated by individual bursts (Fig. 7*A* and *B*). For repetitive theta–gamma stimulation with three to five APs per theta cycle, the rise in steady-state Ca^{2+} concentration measured 2–5 s after stimulation onset was moderate, with a mean concentration that was linearly dependent on the number of APs per gamma cycle (slope 50 ± 2 nM AP^{-1}; Fig. 7*C*).

Furthermore, the amplitude-weighted average decay time constant τ_w after termination of repetitive-burst stimulation was very similar to that of the Ca^{2+} transient evoked by a single burst (515 ± 58 ms and 493 ± 58 ms for 3 and 5 APs, respectively; Fig. 7*D*). In contrast, for repetitive theta–gamma stimulation with 7 or 10 APs per theta cycle, the rise in steady-state Ca^{2+} concentration was markedly higher, being supra-linearly dependent on the number of APs. Likewise, τ_w after termination of repetitive burst stimulation was significantly prolonged ($\tau_w = 2928 \pm 419$ ms for 10 APs; $n = 8$; $P < 0.01$; Fig. 7*D*). This may indicate non-linearity of Ca^{2+} signalling, e.g. caused by saturation of Ca^{2+} uptake into intracellular stores during repetitive activity. Qualitatively similar results were obtained at near-physiological temperature (Fig. 7*C* and *D*). Thus, physiological theta-burst stimulation with three to five APs per theta cycle leads to a moderate rise in the global Ca^{2+} concentration in BC dendrites that is linearly dependent on AP number, whereas more intense stimulation is required to reach micromolar Ca^{2+} concentrations and to shift Ca^{2+} signalling into a non-linear regime.

Discussion

The main findings of the present paper are that the proximal apical dendrites of BCs show high endogenous buffer capacity, small AP-induced Ca^{2+} transients, and relatively slow Ca^{2+} extrusion. A large proportion of the endogenous buffers appears to be fixed, whereas the contribution of mobile buffers is minimal. Owing to the high Ca^{2+} buffer capacitance and the relatively slow extrusion, Ca^{2+} transients decay slowly and summate efficiently. Thus, although BCs are coincidence detectors

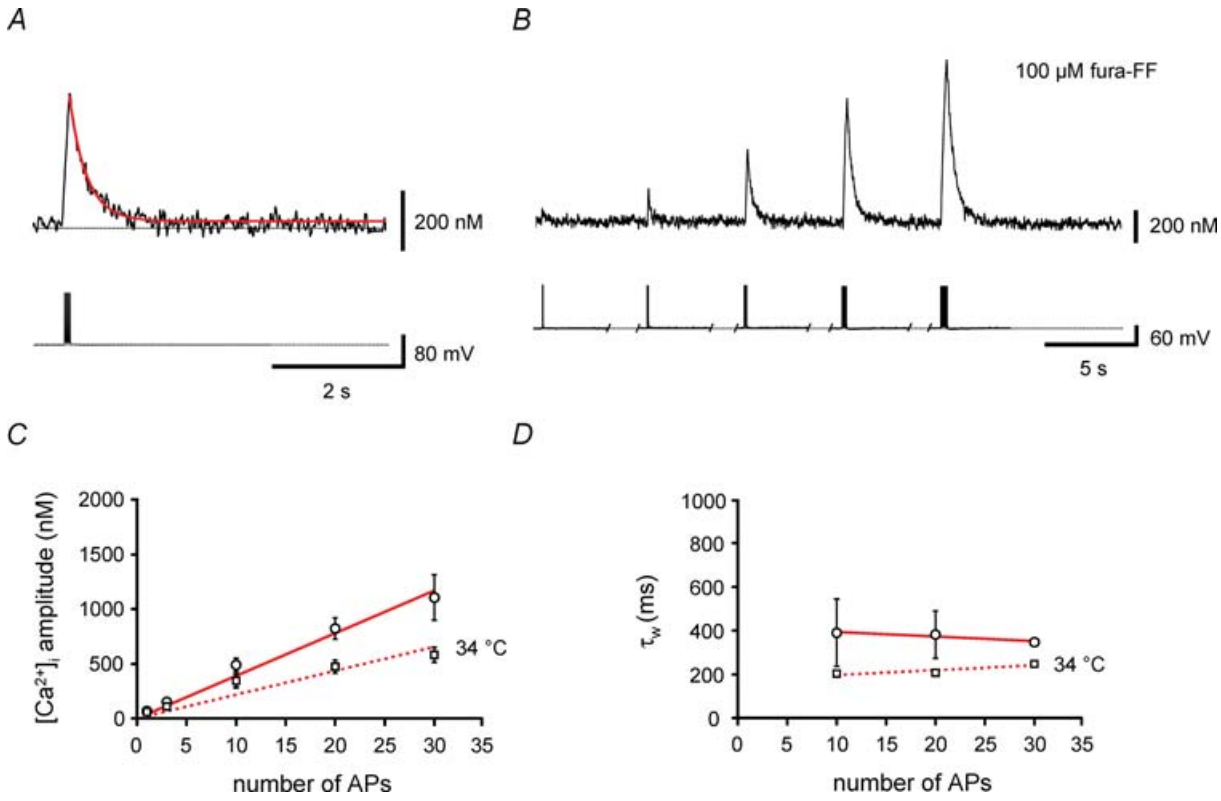

Figure 6. Direct measurement of the amplitude of Ca^{2+} transients and the Ca^{2+} extrusion rate with the low-affinity indicator fura-FF

A and *B*, Ca^{2+} transients recorded in the proximal apical dendrite of a BC filled with 100 μM fura-FF. Upper traces, average Ca^{2+} transients (mean of 10 sweeps); lower traces, corresponding APs evoked by brief current pulses. *A*, Ca^{2+} transients evoked by a 100 Hz train of 10 APs; *B*, Ca^{2+} transients evoked by a single AP or 100 Hz trains of 3, 10, 20 and 30 APs. *C*, plot of peak amplitude of Ca^{2+} transients against the number of APs. ○, data obtained at 22–24°C; □, measurements taken at 34°C. Continuous and dashed lines represent the results of linear regression analysis of the two data sets, yielding steepness values of 39 nM AP^{-1} and 22 nM AP^{-1}, respectively. *D*, plot of amplitude-weighted decay time constant (τ_w) of the Ca^{2+} transients against the number of APs. Data for 1 and 3 APs were omitted, because decay time constants could not be measured reliably. Note that τ_w is almost independent of the number of APs used as stimulus. ○, data obtained at 22–24°C; □, measurements taken at 34°C. Continuous and dashed lines represent the results of linear regression, yielding steepness values of −2.2 ms AP^{-1} and 2.2 ms AP^{-1}, respectively. Data from 7 BCs (22–24°C) and 12 BCs (34°C) filled with 100 μM fura-FF.

at the level of synaptic currents and potentials (Geiger *et al.* 1997; Galarreta & Hestrin, 2001), they are integrators at the level of global Ca^{2+} signals.

Comparison of Ca^{2+} buffering in BCs with that in other cell types

In comparison to other cell types, BCs show a high endogenous Ca^{2+}-binding ratio and a small amplitude of dendritic Ca^{2+} transients. Loading experiments reveal that the endogenous Ca^{2+}-binding ratio in the proximal apical dendrites of BCs is ∼200, and measurements with fura-FF indicate that the amplitude of the unperturbed Ca^{2+} transients is ∼40 nM. In contrast, in the dendrites of principal cells the Ca^{2+}-binding ratio is lower and the amplitude of the Ca^{2+} transients is higher, in both the neocortex ($\kappa_S = 120$ and $A = 260$ nM in layer 5 neocortical pyramidal neurons, Helmchen *et al.* 1996; $\kappa_S = 110$ and $A = 190$–240 nM in layer 2/3 pyramidal neurons; Koester & Sakmann, 2000) and the hippocampus ($\kappa_S = 60$–180 and $A = 150$–240 nM in hippocampal CA1 pyramidal neuron dendrites, Helmchen *et al.* 1996; $\kappa_S = 27$ in CA1 pyramidal neuron dendrites, Rozsa *et al.* 2004; $\kappa_S = 20$ and $A = 1500$–1700 nM in CA1 pyramidal neuron spines, Sabatini *et al.* 2002).

Ca^{2+} signalling in BCs also appears to be distinct from that of other interneuron subtypes examined previously. In hippocampal GABAergic interneurons in culture, the

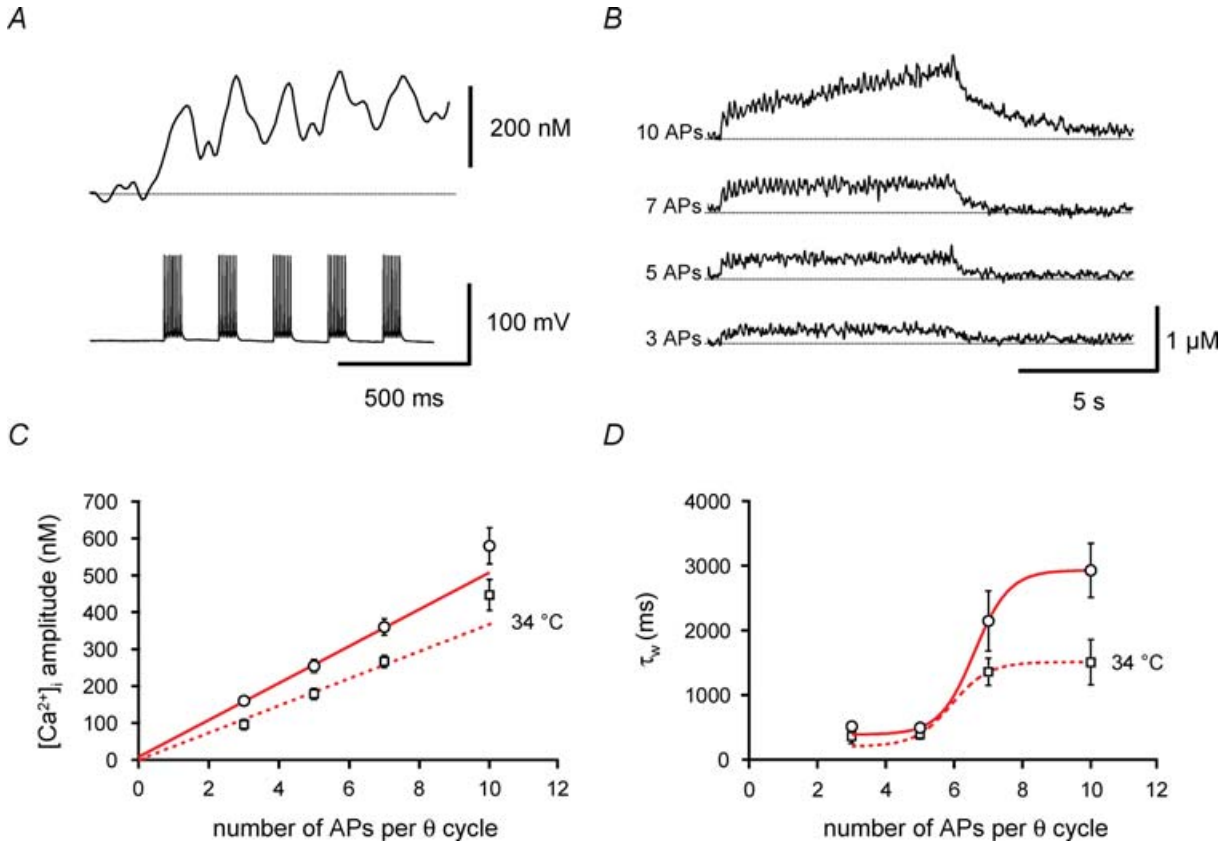

Figure 7. Switch from linear to supralinear Ca^{2+} signalling during repetitive theta-burst stimulation
A and *B*, Ca^{2+} transients recorded in the proximal apical dendrite of a BC filled with 100 μM fura-FF. *A*, expanded view of Ca^{2+} transients evoked at the onset of repetitive 100 Hz burst stimulation. The number of APs per burst was 7, and the burst repetition frequency was 5 Hz. Upper trace, average Ca^{2+} transient; lower trace, corresponding APs evoked by brief current pulses. *B*, Ca^{2+} transients evoked by repetitive 100 Hz burst stimulation for 8 s with 3, 5, 7 or 10 APs per burst (as indicated on the left of each trace). The burst repetition frequency was 5 Hz. Traces of Ca^{2+} transients in *A* and *B* are averages of 5 individual sweeps. *C*, plot of mean amplitude of Ca^{2+} transients against the number of APs. Amplitudes were measured 2–5 s after stimulation onset. ○, data obtained at 22–24°C; □, measurements taken at 34°C. Continuous and dashed lines represent the results of linear regression of the data points for 3, 5 and 7 APs, yielding steepness values of 50 nM AP^{-1} and 37 nM AP^{-1}, respectively. *D*, plot of amplitude-weighted average decay time constant (τ_w) of the Ca^{2+} transients after the end of stimulation against the number of APs per burst. Note that τ_w is similar for 3 and 5 APs, but increases markedly for a larger number of APs. ○, data obtained at 22–24°C; □, measurements taken at 34°C. Continuous and dashed curves represent non-linear fits with a Boltzmann function with a constant offset constrained to the mean τ_w for a single burst of 10 APs. Data from 8 BCs (22–24°C) and 7 BCs (34°C) filled with 100 μM fura-FF.

endogenous Ca^{2+}-binding ratio (∼150) is similar to that in BCs, but the amplitude of the Ca^{2+} transients evoked by 3 ms pulses (presumably evoking a single action potential) is larger (> 100 nM; Lee *et al.* 2000*a*). Likewise, in bitufted interneurons in the neocortex, which presumably express the peptide somatostatin, the endogenous Ca^{2+}-binding ratio is comparable (∼300) to that in BCs, but the amplitude of the Ca^{2+} transients is markedly larger (140 nM; Kaiser *et al.* 2001). Finally, in CA1 stratum radiatum interneurons a lower Ca^{2+}-binding ratio of 71 was estimated (Rozsa *et al.* 2004). Thus, our results and the previous data support the view that interneurons show a higher Ca^{2+} buffer capacity than principal neurons, but also suggest differences between interneuron subtypes.

Shaping of local and global Ca^{2+} signalling by endogenous buffering properties

How does efficient Ca^{2+} buffering in BCs affect the local Ca^{2+} signals near transiently activated Ca^{2+}-permeable AMPARs (Koh *et al.* 1995) or voltage-gated Ca^{2+} channels (Bucurenciu *et al.* 2008) and the global Ca^{2+} signals in dendrites or presynaptic terminals? For local Ca^{2+} transients examined near the source on the time scale of milliseconds, the early peak phase of the transient is expected to be only minimally affected by endogenous buffers, whereas the later sustained phase will be strongly attenuated according to the high Ca^{2+}-binding ratio. Fixed buffers will have an even smaller effect on the peak amplitude than mobile buffers, because fixed buffers will be saturated near the source, whereas mobile buffers are rapidly replenished (Neher, 1998; Meinrenken *et al.* 2002, 2003). In contrast, for global Ca^{2+} transients examined further away from the source and at a slower time scale, Ca^{2+} buffers will reduce the amplitude and prolong the decay phase of the Ca^{2+} transient, because the buffers will slowly release previously bound Ca^{2+}. Thus, the abundance of immobile buffers in BCs will sharpen the time course of local Ca^{2+} signals and at the same time prolong the decay of global Ca^{2+} signals. Concomitantly, the buffering properties will reduce the spatial extent of nanodomains around the Ca^{2+} source (Goldberg *et al.* 2003*a*). Thus, the abundance of fixed buffers will confer unique spatiotemporal properties on Ca^{2+} signalling in BC dendrites and presynaptic terminals.

Possible implications for synaptic transmission and plasticity

Shaping of Ca^{2+} signals in BCs by endogenous buffers may be important for the function of both input and output synapses of BCs. Accumulating evidence suggests that glutamatergic input synapses of BCs exhibit long-term potentiation (LTP; Alle *et al.* 2001; Perez *et al.* 2001; Kullmann & Lamsa, 2007). However, it is controversial which associative protocols are most efficient for LTP induction (Alle *et al.* 2001; Perez *et al.* 2001; Kullmann & Lamsa, 2007). Our results imply that the induction rules of synaptic plasticity at glutamatergic principal neuron–interneuron synapses may be complex. The associative nature and the Ca^{2+} dependence of LTP may suggest that both a local Ca^{2+} increase through Ca^{2+}-permeable AMPARs and a global Ca^{2+} increase triggered by APs may be necessary for LTP induction. If pre- and postsynaptic activity were precisely coincident, synaptic efficacy may be unchanged, because Ca^{2+}-permeable AMPARs are rapidly blocked by intracellular polyamines (Kullmann & Lamsa, 2007). In contrast, if the coincidence of pre- and postsynaptic activity is looser (Alle *et al.* 2001; Perez *et al.* 2001), AMPAR-mediated and AP-induced Ca^{2+} transients will summate efficiently (see Rozsa *et al.* 2004). Similarly, a prolonged train of large but subthreshold EPSPs may generate large intracellular Ca^{2+} signals. In both scenarios, the abundance of immobile buffers in BCs will prolong the decay of Ca^{2+} transients, widening the temporal window of LTP induction.

If the properties of Ca^{2+} buffering in BC terminals are the same as those in the apical dendrites, the high endogenous binding ratio will have implications for the efficiency and temporal precision of transmitter release at GABAergic BC output synapses (Bartos *et al.* 2007). In BC synaptic terminals, immobile buffers will have little effect on local Ca^{2+} transients at the peak, but reduce the Ca^{2+} concentration at later times. Thus, the buffering properties of BCs appear to be optimal to maximize the ratio of synchronous over asynchronous release. Together with the tight coupling of presynaptic Ca^{2+} channels and the Ca^{2+} sensors of exocytosis at this synapse (Bucurenciu *et al.* 2008), this would explain why fast-spiking, parvalbumin-expressing BCs release transmitter efficiently and with high temporal precision (Kraushaar & Jonas, 2000; Hefft & Jonas, 2005; Bucurenciu *et al.* 2007). Thus, Ca^{2+} buffering properties may contribute to the efficiency and temporal precision of BC-mediated inhibition in hippocampal microcircuits (Pouille & Scanziani, 2004).

References

Alle H, Jonas P & Geiger JRP (2001). PTP and LTP at a hippocampal mossy fiber-interneuron synapse. *Proc Natl Acad Sci U S A* **98**, 14708–14713.

Aponte Y, Lien CC, Bischofberger J & Jonas P (2006*a*). Dendritic calcium signaling in fast-spiking hippocampal basket cells. *Abstr Soc Neurosci* 337.12.

Aponte Y, Lien CC, Reisinger E & Jonas P (2006*b*). Hyperpolarization-activated cation channels in fast-spiking interneurons of rat hippocampus. *J Physiol* **574**, 229–243.

Bartos M, Vida I & Jonas P (2007). Synaptic mechanisms of synchronized gamma oscillations in inhibitory interneuron networks. *Nat Rev Neurosci* **8**, 45–56.

Bragin A, Jandó G, Nádasdy Z, Hetke J, Wise K & Buzsáki G (1995). Gamma (40–100 Hz) oscillation in the hippocampus of the behaving rat. *J Neurosci* **15**, 47–60.

Bucurenciu I, Kulik A, Schwaller B, Frotscher M & Jonas P (2008). Nanodomain coupling between Ca^{2+} channels and Ca^{2+} sensors promotes fast and efficient transmitter release at a cortical GABAergic synapse. *Neuron* **57**, 536–545.

Cobb SR, Buhl EH, Halasy K, Paulsen O & Somogyi P (1995). Synchronization of neuronal activity in hippocampus by individual GABAergic interneurons. *Nature* **378**, 75–78.

Collin T, Chat M, Lucas MG, Moreno H, Racay P, Schwaller B, Marty A & Llano I (2005). Developmental changes in parvalbumin regulate presynaptic Ca^{2+} signaling. *J Neurosci* **25**, 96–107.

Csicsvari J, Jamieson B, Wise KD & Buzsáki G (2003). Mechanisms of gamma oscillations in the hippocampus of the behaving rat. *Neuron* **37**, 311–322.

Efron B & Tibshirani RJ (1998). *An Introduction to the Bootstrap*. Chapman & Hall/CRC, Boca Raton, USA.

Freund TF & Buzsáki G (1996). Interneurons of the hippocampus. *Hippocampus* **6**, 347–470.

Galarreta M & Hestrin S (2001). Spike transmission and synchrony detection in networks of GABAergic interneurons. *Science* **292**, 2295–2299.

Geiger JRP, Bischofberger J, Vida I, Fröbe U, Pfitzinger S, Weber HJ, Haverkampf K & Jonas P (2002). Patch-clamp recording in brain slices with improved slicer technology. *Pflugers Arch* **443**, 491–501.

Geiger JRP, Lübke J, Roth A, Frotscher M & Jonas P (1997). Submillisecond AMPA receptor-mediated signaling at a principal neuron-interneuron synapse. *Neuron* **18**, 1009–1023.

Geiger JRP, Melcher T, Koh DS, Sakmann B, Seeburg PH, Jonas P & Monyer H (1995). Relative abundance of subunit mRNAs determines gating and Ca^{2+} permeability of AMPA receptors in principal neurons and interneurons in rat CNS. *Neuron* **15**, 193–204.

Goldberg JH, Tamas G, Aronov D & Yuste R (2003*a*). Calcium microdomains in aspiny dendrites. *Neuron* **40**, 807–821.

Goldberg JH, Yuste R & Tamas G (2003*b*). Ca^{2+} imaging of mouse neocortical interneurone dendrites: contribution of Ca^{2+}-permeable AMPA and NMDA receptors to subthreshold Ca^{2+} dynamics. *J Physiol* **551**, 67–78.

Grynkiewicz G, Poenie M & Tsien RY (1985). A new generation of Ca^{2+} indicators with greatly improved fluorescence properties. *J Biol Chem* **260**, 3440–3450.

Hefft S & Jonas P (2005). Asynchronous GABA release generates long-lasting inhibition at a hippocampal interneuron-principal neuron synapse. *Nat Neurosci* **8**, 1319–1328.

Helmchen F & Tank DW (2005). A single-compartment model of calcium dynamics in nerve terminals and dendrites. In *Imaging in Neuroscience and Development*, ed. Yuste R & Konnerth A, pp. 265–275. CSHL Press, Cold Spring Harbour, USA.

Helmchen F, Borst JGG & Sakmann B (1997). Calcium dynamics associated with a single action potential in a CNS presynaptic terminal. *Biophys J* **72**, 1458–1471.

Helmchen F, Imoto K & Sakmann B (1996). Ca^{2+} buffering and action potential-evoked Ca^{2+} signaling in dendrites of pyramidal neurons. *Biophys J* **70**, 1069–1081.

Jonas P, Bischofberger J, Fricker D & Miles R (2004). Interneuron diversity series: Fast in, fast out – temporal and spatial signal processing in hippocampal interneurons. *Trends Neurosci* **27**, 30–40.

Kaiser KMM, Zilberter Y & Sakmann B (2001). Back-propagating action potentials mediate calcium signalling in dendrites of bitufted interneurons in layer 2/3 of rat somatosensory cortex. *J Physiol* **535**, 17–31.

Koester HJ & Sakmann B (2000). Calcium dynamics associated with action potentials in single nerve terminals of pyramidal cells in layer 2/3 of the young rat neocortex. *J Physiol* **529**, 625–646.

Koh D-S, Geiger JRP, Jonas P & Sakmann B (1995). Ca^{2+}-permeable AMPA and NMDA receptor channels in basket cells of rat hippocampal dentate gyrus. *J Physiol* **485**, 383–402.

Kraushaar U & Jonas P (2000). Efficacy and stability of quantal GABA release at a hippocampal interneuron-principal neuron synapse. *J Neurosci* **20**, 5594–5607.

Kullmann DM & Lamsa KP (2007). Long-term synaptic plasticity in hippocampal interneurons. *Nat Rev Neurosci* **8**, 687–699.

Lee SH, Rosenmund C, Schwaller B & Neher E (2000*a*). Differences in Ca^{2+} buffering properties between excitatory and inhibitory hippocampal neurons from the rat. *J Physiol* **525**, 405–418.

Lee SH, Schwaller B & Neher E (2000*b*). Kinetics of Ca^{2+} binding to parvalbumin in bovine chromaffin cells: implications for $[Ca^{2+}]$ transients of neuronal dendrites. *J Physiol* **525**, 419–432.

Lei S & McBain CJ (2002). Distinct NMDA receptors provide differential modes of transmission at mossy fiber-interneuron synapses. *Neuron* **33**, 921–933.

Meinrenken CJ, Borst JGG & Sakmann B (2002). Calcium secretion coupling at calyx of Held governed by nonuniform channel-vesicle topography. *J Neurosci* **22**, 1648–1667.

Meinrenken CJ, Borst JGG & Sakmann B (2003). Local routes revisited: the space and time dependence of the Ca^{2+} signal for phasic transmitter release at the rat calyx of Held. *J Physiol* **547**, 665–689.

Miles R (1990). Synaptic excitation of inhibitory cells by single CA3 hippocampal pyramidal cells of the guinea-pig *in vitro*. *J Physiol* **428**, 61–77.

Müller M, Felmy F, Schwaller B & Schneggenburger R (2007). Parvalbumin is a mobile presynaptic Ca^{2+} buffer in the calyx of Held that accelerates the decay of Ca^{2+} and short-term facilitation. *J Neurosci* **27**, 2261–2271.

Neher E (1995). The use of fura-2 for estimating Ca buffers and Ca fluxes. *Neuropharmacology* **34**, 1423–1442.

Neher E (1998). Usefulness and limitations of linear approximations to the understanding of Ca^{++} signals. *Cell Calcium* **24**, 345–357.

Neher E & Augustine GJ (1992). Calcium gradients and buffers in bovine chromaffin cells. *J Physiol* **450**, 273–301.

Normann C, Peckys D, Schulze CH, Walden J, Jonas P & Bischofberger J (2000). Associative long-term depression in the hippocampus is dependent on postsynaptic N-type Ca^{2+} channels. *J Neurosci* **20**, 8290–8297.

Penttonen M, Kamondi A, Acsády L & Buzsáki G (1998). Gamma frequency oscillation in the hippocampus of the rat: intracellular analysis *in vivo*. *Eur J Neurosci* **10**, 718–728.

Perez Y, Morin F & Lacaille JC (2001). A hebbian form of long-term potentiation dependent on mGluR1a in hippocampal inhibitory interneurons. *Proc Natl Acad Sci U S A* **98**, 9401–9406.

Pouille F & Scanziani M (2004). Routing of spike series by dynamic circuits in the hippocampus. *Nature* **429**, 717–723.

Rozsa B, Zelles T, Vizi ES & Lendvai B (2004). Distance-dependent scaling of calcium transients evoked by backpropagating spikes and synaptic activity in dendrites of hippocampal interneurons. *J Neurosci* **24**, 661–670.

Rudy B & McBain CJ (2001). Kv3 channels: voltage-gated K^+ channels designed for high-frequency repetitive firing. *Trends Neurosci* **24**, 517–526.

Sabatini BL, Oertner TG & Svoboda K (2002). The life cycle of Ca^{2+} ions in dendritic spines. *Neuron* **33**, 439–452.

Schiller J, Helmchen F & Sakmann B (1995). Spatial profile of dendritic calcium transients evoked by action potentials in rat neocortical pyramidal neurones. *J Physiol* **487**, 583–600.

Schmidt H, Brown EB, Schwaller B & Eilers J (2003). Diffusional mobility of parvalbumin in spiny dendrites of cerebellar Purkinje neurons quantified by fluorescence recovery after photobleaching. *Biophys J* **84**, 2599–2608.

Schwaller B, Meyer M & Schiffmann S (2002). 'New' functions for 'old' proteins: the role of the calcium-binding proteins calbindin D-28k, calretinin and parvalbumin, in cerebellar physiology. Studies with knockout mice. *Cerebellum* **1**, 241–258.

Sík A, Hájos N, Gulácsi A, Mody I & Freund TF (1998). The absence of a major Ca^{2+} signaling pathway in GABAergic neurons of the hippocampus. *Proc Natl Acad Sci U S A* **95**, 3245–3250.

Sloviter RS, Zappone CA, Harvey BD, Bumanglag AV, Bender RA & Frotscher M (2003). 'Dormant basket cell' hypothesis revisited: relative vulnerabilities of dentate gyrus mossy cells and inhibitory interneurons after hippocampal status epilepticus in the rat. *J Comp Neurol* **459**, 44–76.

Somogyi P & Klausberger T (2005). Defined types of cortical interneurone structure space and spike timing in the hippocampus. *J Physiol* **562**, 9–26.

Toth K, Suares G, Lawrence JJ, Philips-Tansey E & McBain CJ (2000). Differential mechanisms of transmission at three types of mossy fiber synapse. *J Neurosci* **20**, 8279–8289.

Acknowledgements

We thank Dr Iancu Bucurenciu for critically reading the manuscript, and Selma Becherer, Margit Northemann and Karin Winterhalter for technical assistance. Supported by the Deutsche Forschungsgemeinschaft (BI 642/2, Sonderforschungsbereich 505, Sonderforschungsbereich 780, and Leibniz program).

Author's present address

Y. Aponte: Janelia Farm Research Campus, HHMI, 19700 Helix Drive, Ashburn, VA 20147, USA.